ACS OMEGA

http://pubs.acs.org/journal/acsodf

Article

Contribution of Na/K Doping to the Activity and Mechanism of Low-Temperature COS Hydrolysis over TiO_2-Al_2O_3 Based Catalyst in Blast Furnace Gas

Yiliang Liu, Peng Wu, Kai Shen,* Yaping Zhang,* Guobo Li, and Bo Li

Cite This: *ACS Omega* 2022, 7, 13299−13312

Read Online

ACCESS | Metrics & More | Article Recommendations

ABSTRACT: As an organic sulfur pollutant generated in blast furnace gas, carbonyl sulfide (COS) has attracted more attention due to its negative effects on the environment and economy. The TiO_2-Al_2O_3 composite metal oxide ($Ti_{0.5}Al$) with uniformly dispersed particles was prepared by the co-precipitation method. And on this basis, a series of Na/K-doped catalysts were prepared separately. The activity evaluation results showed that the introduction of Na/K significantly improved the low-temperature COS hydrolysis activity, which exhibited a COS conversion of 98% and H_2S yield of 95% at 75 °C with 24,000 h^{-1}. And K showed a better promoting effect than Na. Brunauer−Emmett−Teller (BET) results revealed the increased mesopore proportion of Na/K-modified catalysts. X-ray diffraction (XRD) and scanning electron microscopy (SEM) showed that Na and K formed prismatic and nanorod-like structures, respectively. More weakly basic sites with enhanced intensity and decreased O_{ads}/O_{lat} content contributed to the excellent catalytic activity, as certified by the results of CO_2 temperature-programmed desorption (CO_2-TPD) and X-ray photoelectron spectroscopy (XPS). It was also proposed that the decrease of weakly basic sites ultimately deactivated catalyst activity. In situ diffuse reflectance infrared Fourier transform spectroscopy (DRIFTS) showed that the introduction of Na/K enhanced the dissociation of H_2O, and the generated abundant hydroxyl groups promoted the adsorption of COS and formed surface transition species, such as $HSCO_2^-$ and HCO_3^-.

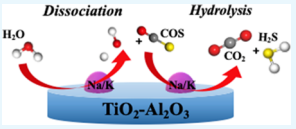

1. INTRODUCTION

Carbonyl sulfide (COS) widely exists as the byproduct gas of the steel industry, such as blast furnace gas, coke oven gas, and converter gas. The environmental pollution, such as acid rain, and serious chemical equipment corrosion caused by COS have aroused widespread attention from researchers.[1−4] Research on the corresponding COS elimination technology possessed significant practical value in environmental protection and industrial utilization. Till now, adsorption,[5] hydrogenation conversion,[6] and catalytic hydrolysis[7,8] are the commonly used methods for COS removal in the industry. Adsorption is an effective method for purifying low-concentration sulfur-containing gas, but the regeneration of exhausted adsorbent requires a higher temperature and complicated process. Hydrogenation requires an additional source of hydrogen and is prone to methanation side reactions at operating temperatures of 280−400 °C.[9] The catalytic hydrolysis technology has been recognized to be the most promising method for COS removal due to its mild reaction condition and high conversion efficiency.[10] At the same time, the hydrolysate H_2S can be easily removed due to its relative acidity and higher polarity. The catalytic hydrolysis reaction equation is

$$COS\ (g) + H_2O\ (g) \rightarrow H_2S\ (g) + CO_2\ (g) \quad (1)$$

So far, researches on hydrolysis catalysts are mainly based on γ-Al_2O_3,[11,12] activated carbon (AC),[13] and hydrotalcite-like compounds (HTLCs).[2,14] However, ACs mainly rely on their loaded active components for hydrolysis,[15] and the special structure of HTLCs is not suitable for industrial applications. γ-Al_2O_3 stands out among these catalysts due to its inherent hydrolytic properties. Besides, the high surface activity and thermal stability are also advantages of γ-Al_2O_3. However, the anti-sulfate poisoning ability of this catalyst is very weak.[16] Studies have shown that under the same condition of sulfate poisoning, the activity of TiO_2 is reduced to a lesser extent than that of γ-Al_2O_3,[17] indicating that TiO_2 has the ability to resist sulfate poisoning.[18] Therefore, TiO_2-Al_2O_3 composite metal oxides are worth to be investigated as COS hydrolysis catalysts. However, only a few studies on the modification of γ-Al_2O_3 by Ti have been reported in the literature. Liu et al.[19] found that the addition of Ti catalysts exhibited high catalytic activity at moderate temperatures (150−350 °C), while there were no remarkable influences on the catalytic activity at a low temperature (40 °C) as certified by Liang et al.[20] Considering that the blast furnace gas temperature is in the range of 70−120 °C, it is obvious that the current Ti-modified γ-Al_2O_3

Received: February 17, 2022
Accepted: March 22, 2022
Published: April 6, 2022

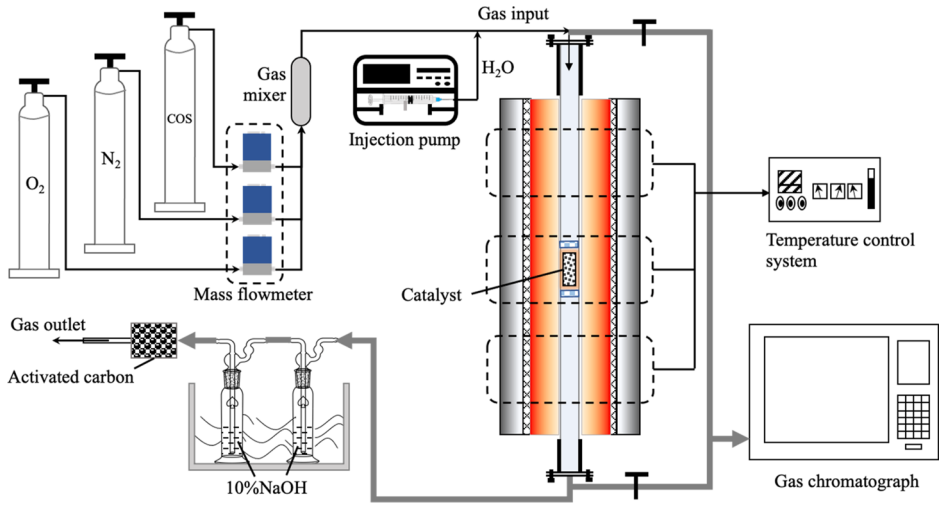

Figure 1. Catalytic activity evaluation system.

catalysts cannot achieve high catalytic activity at this temperature, which poses unavoidable obstacles and additional costs to industrial applications.[10] Therefore, achieving the low-temperature catalytic activity of TiO_2-Al_2O_3 composite catalysts becomes the focus of further research.

Loading active components is an effective and the most common way to improve catalytic activity. For example, Jin et al.[12] prepared Ni-Al_2O_3 catalysts with a COS conversion above 95% at 80 °C with 6,000 h^{-1}. Nimthuphariyha et al.[21] found that the addition of Pt and Ba on Al_2O_3 helped to stabilize the catalytic hydrolysis activity of COS with a weight hourly space velocity (WHSV) of 7000 h^{-1} at 150−250 °C. George[22] reported that impregnation with NaOH increased the rate of COS hydrolysis of Al_2O_3 by a factor of about 25. Cao et al.[23] recorded that the K/Mo-Al_2O_3 catalyst exhibited high COS removal efficiency at 80 °C. Notably, COS hydrolysis is not identified as a redox reaction, so strong electron-active and redox-capable transition metals and rare earth metals may lead to the over-oxidizing reaction of COS.[15,17,24,25] In addition, previous studies confirmed that COS hydrolysis is a typical base-catalyzed reaction. The establishment and enhancement of alkaline sites are the key to improve the hydrolytic activity.[15] Accordingly, alkali metals are considered to be the most effective active components for improving the basic sites on the catalyst surface.[26] Therefore, the low-temperature activity of TiO_2-Al_2O_3 composite catalysts can be improved by introducing alkali metals, which is still lacking in current research.

In this paper, a TiO_2-Al_2O_3 composite carrier with homogeneous components was prepared by the co-precipitation method for the elimination of COS at low temperatures (50−150 °C). The catalysts were modified by doping with alkali metals (Na, K) to improve the low-temperature hydrolysis efficiency and deeply investigate the role of alkali metals in this process. The relationship between H_2S yield and long-term hydrolytic activity was analyzed. The effects of alkali metals on the catalyst structure, surface alkalinity, and reaction intermediates are discussed. The research results of this paper can provide a theoretical basis for blast furnace gas hydrolysis catalysts.

2. MATERIALS AND METHODS

2.1. Catalyst Preparation. The TiO_2-Al_2O_3 composite oxide was prepared by a co-precipitation method. Under the action of ice-water bath and vigorous stirring, calculated amounts of $Al(NO_3)_3{\cdot}9H_2O$ and $TiCl_4$ solution were dissolved and mixed in deionized water. An appropriate amount of ammonia was added dropwise to the obtained solution with constant stirring until the pH of the mixture was controlled to 10 so as to obtain a white precipitate. The sediment was allowed to stand and age for 24 h at room temperature. And then the supernatant was filtered off, and the white precipitate was washed with deionized water until the chloride ion disappeared, which then was dried in an oven at 105 °C for 12 h. Finally, the precursors were calcined in N_2 gas at 600 °C for 5 h and named $Ti_{0.5}Al$ (Ti/Al = 0.50, molar ratio).

The corresponding masses of Na_2CO_3, K_2CO_3, and the prepared $Ti_{0.5}Al$ carrier were weighed according to the element molar ratio of the prepared samples (Na/Al = K/Al = 0.05−0.30, molar ratio). The calculated load components were dissolved in a certain amount of deionized water, respectively, and then were added to the weighed $Ti_{0.5}Al$ carrier to make a mixed solution; the mixed solution was uniformly stirred at 25 °C for 2 h and then heated to 85 °C with continuous stirring until the moisture basically evaporated. It was then placed in an oven at 105 °C to dry for 12 h and calcined in a muffle furnace at 500 °C for 5 h. After cooling, catalysts with different loading components were obtained.

2.2. Catalyst Characterization. In this article, the Brunauer−Emmett−Teller (BET) test used the ASAP2020 analyzer (Micromeritics, USA) to obtain the pore parameters of the catalysts, including the specific surface area, total pore volume, average pore diameter, etc. Prior to the analysis, the catalysts were degassed at 300 °C for 5 h in the vacuum state.

The microscopic surface morphology and structure of the catalysts were observed by scanning electron microscopy (SEM) on a Zeiss Sigma 300 (Zeiss, Germany).

X-ray diffraction (XRD) was used to obtain information about the material composition and crystal phase structure of the catalysts by using a SmartLab X-ray diffractometer (Rigaku, Japan).

The surface alkalinity of the catalysts was measured by CO_2 temperature-programmed desorption (CO_2-TPD) with the FINSORB-3010 analyzer (Finetec Instruments, China). After

https://doi.org/10.1021/acsomega.2c00968
ACS Omega 2022, 7, 13299−13312

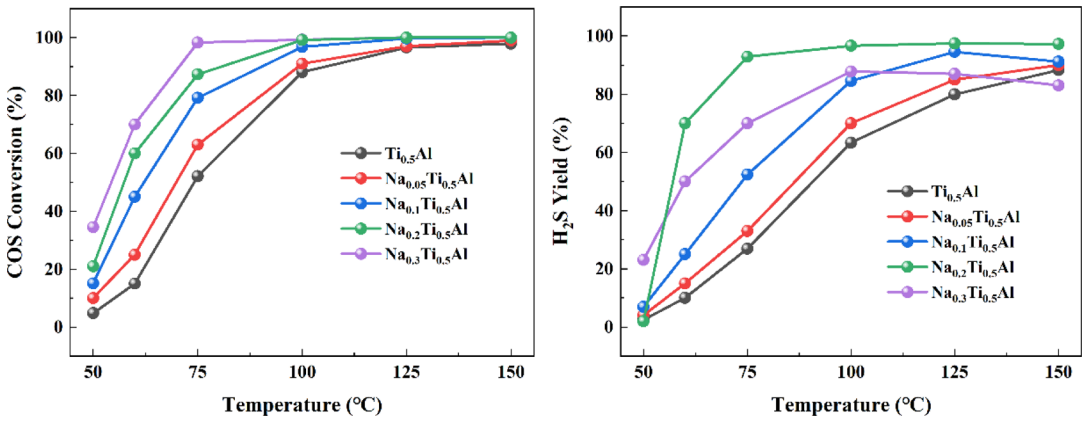

Figure 2. The catalytic performance of COS hydrolysis over $Na_xTi_{0.5}Al$ ($[COS]_{in}$: 200 ppm; GHSV: 24,000 h^{-1}; 49% RH).

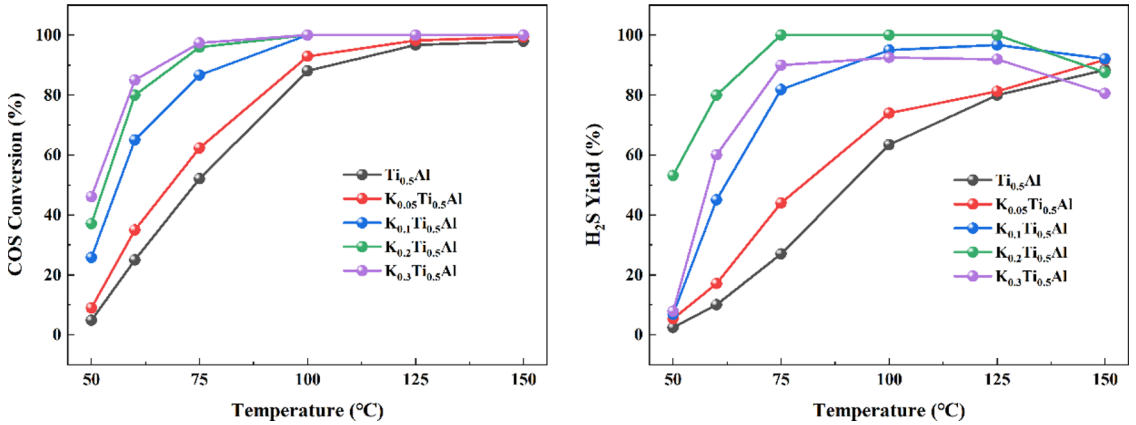

Figure 3. The catalytic performance of COS hydrolysis over $K_xTi_{0.5}Al$ ($[COS]_{in}$: 200 ppm; GHSV: 24,000 h^{-1}; 49% RH).

being pretreated in He flow at 300 °C for 1 h, the catalysts were treated with 1% CO_2/He at 20 mL/min for 40 min at room temperature and then were purged with He during heating from room temperature to 800 °C with a heating rate of 10 °C/min.

X-ray photoelectron spectroscopy (XPS) was used to analyze the valence states of surface elements. A K-Alpha X-ray electron spectrometer (Thermo Scientific, USA) was used to analyze the catalysts by XPS. Binding energies (BEs) were calibrated using the C 1s peak of contaminant carbon at 284.8 eV.

In situ diffuse reflectance infrared Fourier transform spectroscopy (in situ DRIFTS) experiments were carried out via a Nicolet 6700 spectrometer (Thermo Scientific, USA) to explore the COS/H_2O adsorption behaviors and reaction mechanism on the catalysts. Before each measurement, the sample was purged with N_2 at 300 °C for 1 h. The spectral range was 700−4000 cm^{-1}.

2.3. Catalytic Activity Test. COS catalytic hydrolysis activity tests were carried out in a fixed-bed reactor (i.d. 18 mm) at a given temperature (50−150 °C). The catalyst was loaded into a quartz tube with 0.5 mL with a gas hourly space velocity (GHSV) of 24,000 h^{-1}. Typically, the total gas flow rate was 200 mL/min, which was premixed in a gas mixer to obtain the simulated gas of 200 ppm of COS and a given content of water vapor (49% RH) and balanced by N_2. Water vapor was introduced by a water saturator system. Then, the mixed gas went into the reactor. The COS and H_2S concentrations were continually monitored by a gas chromatograph (GC-9860-5C-NJ). The catalytic activity evaluation system is shown in Figure 1.

The conversion of COS was calculated by

$$\text{COS conversion} = \frac{[COS]_{in} - [COS]_{out}}{[COS]_{in}} \times 100\% \quad (2)$$

where $[COS]_{in}$ and $[COS]_{out}$ are the concentration of COS in the inlet gas and outlet gas, respectively.

The H_2S yield was also considered and calculated by

$$H_2S\ \text{yield} = \frac{[H_2S]_{out}}{[COS]_{in} - [COS]_{out}} \times 100\% \quad (3)$$

where $[H_2S]_{out}$ is the concentration of H_2S in the outlet gas.

The adsorption of H_2S was calculated by

$$H_2S\ \text{adsorption} = \frac{[H_2S]_{in} - [H_2S]'_{out}}{[H_2S]_{in}} \times 100\% \quad (4)$$

where $[H_2S]'_{out}$ is the concentration of H_2S in the outlet gas.

3. RESULTS AND DISCUSSION

3.1. Catalytic Performance of COS Hydrolysis. *3.1.1. Effect of the Reaction Temperature.* The effect of Na/K doping on the hydrolysis efficiency of COS was investigated by activity evaluation tests. Figures 2 and 3 illustrate the hydrolysis effects of Na and K at various temperatures. It can be seen from the activity curves that the catalyst without the addition of alkali metal had a certain medium-temperature catalytic activity, which was reflected in

https://doi.org/10.1021/acsomega.2c00968
ACS Omega 2022, 7, 13299−13312

the COS conversion of over 80% at 100 °C and even reaching 95% at 125 °C. However, its catalytic activity below 75 °C was relatively poor (less than 50%), indicating the narrow active temperature range. Moreover, the H_2S yield of the unmodified $Ti_{0.5}Al$ catalyst only achieved 27.04% at 75 °C and increased to 88.42% at 150 °C. The activity of Na/K-doped catalysts above 100 °C was still excellent, and the low-temperature activity had been significantly improved. The COS conversion of the $Na_{0.3}Ti_{0.5}Al$ catalyst at 75 °C was raised to 98.32 from 52.14%. And the $K_{0.3}Ti_{0.5}Al$ catalyst further increased the COS conversion from 4.80 to 46.11% at 50 °C. It can be concluded that the promotion effect of Na and K was mainly reflected in the significant improvement of the low-temperature activity of the catalyst, especially K-doped catalysts. The research of Thomas et al.[26] also proved that the catalytic activity of K was better than that of Na. The modification effect of both Na and K doping was reflected not only in the improvement of low temperature activity but also in the greatly enhanced H_2S yield. Compared with $Ti_{0.5}Al$, the best Na-doped catalyst can increase the H_2S yield by two times at 75 °C, and that of K-doped catalyst can be raised by 55% at 50 °C. This meant that the introduction of alkali metals promoted the hydrolysis reaction of COS.

It can also be observed in Figures 2 and 3 that the doping ratio of alkali metal also had a relatively obvious impact on the COS conversion and the H_2S yield. Under the same reaction temperature, the increase of Na/K doping was beneficial to the continuous improvement of COS conversion, while the H_2S yield showed a trend of first increasing and then decreasing (from 30 to 95 to 70%). Since the hydrolysis of COS is a recognized base-catalyzed reaction, it can be reasonablely inferred that the introduction of an appropriate amount of alkali metal can enrich the surface active sites, thereby enhancing the hydrolysis activity. On the contrary, an excessive loading ratio will make the surface too alkaline. The hydrolysate H_2S was captured by the strong surface alkali and then deposited, resulting in a decrease in the measured H_2S yield. It revealed that the appropriate amount of Na/K doping contributed to the COS hydrolysis at low temperatures, while an excessive Na/K content inhibited the long-term progress of the reaction due to the deposition of sulfur species. The optimal doping ratio of Na and K was $Na_{0.2}Ti_{0.5}Al$ and $K_{0.2}Ti_{0.5}Al$, respectively.

It is worth noting that the H_2S yield of some samples decreased above 125 °C, such as $Na_{0.3}Ti_{0.5}Al$ and $K_{0.3}Ti_{0.5}Al$. It was initially speculated that this was due to the fact that H_2S could be adsorbed and oxidized on the catalysts at high temperatures. To further verify this conclusion, the catalysts were tested for H_2S adsorption at different temperatures. As shown in Figure 4, the adsorption of H_2S was hardly observed on $Ti_{0.5}Al$ at lower temperatures. However, when the reaction temperature reached 150 °C, the adsorption of H_2S actually reached about 51%. And the same experimental phenomenon can be observed on $K_{0.2}Ti_{0.5}Al$. It can be speculated that it was precisely due to the adsorption and oxidation of H_2S that the H_2S yield decreased at high temperatures, which was certified by Wei et al.[27] This may cause the catalytic performance of the catalyst to be limited. Therefore, improving the low-temperature activity of the catalyst is beneficial to ensure long-term catalytic performance.

3.1.2. Durability Performance. The durability hydrolysis activities of $Ti_{0.5}Al$ and $K_{0.2}Ti_{0.5}Al$ catalysts were tested in the presence of 200 ppm COS and 0.5% vol O_2 at 100 °C. As shown in Figure 5, COS conversion of unmodified $Ti_{0.5}Al$ decreased from the initial 89.28 to 79.79% after 14 h.

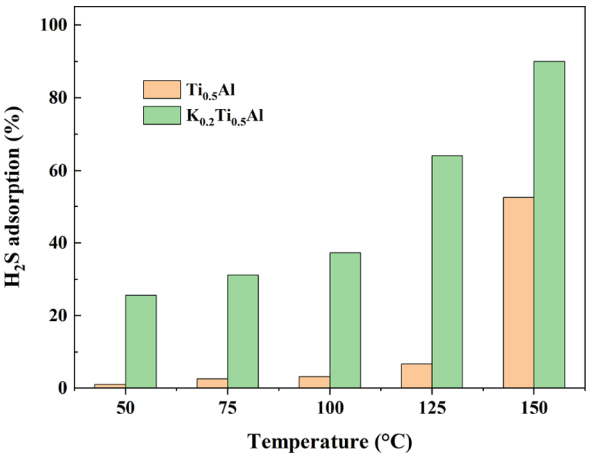

Figure 4. The H_2S adsorption of prepared catalysts ($[H_2S]_{in}$: 200 ppm; GHSV: 24,000 h^{-1}).

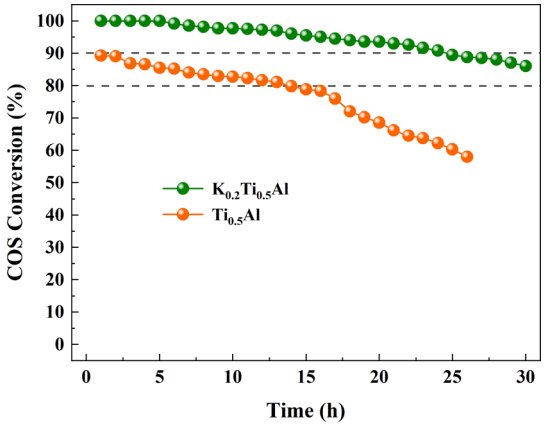

Figure 5. Durability performance of COS hydrolysis on $Ti_{0.5}Al$ and $K_{0.2}Ti_{0.5}Al$ ($[COS]_{in}$: 200 ppm; 0.5% vol O_2; GHSV: 24,000 h^{-1}; 49% RH).

Compared with the $Ti_{0.5}Al$ catalyst, the $K_{0.2}Ti_{0.5}Al$ catalyst exhibited great catalytic durability. Under the condition of O_2, the initial 100% COS conversion of the $K_{0.2}Ti_{0.5}Al$ catalyst was maintained for 5 h. The COS conversion of the $K_{0.2}Ti_{0.5}Al$ catalyst could still be maintained at around 85% for 30 h. It could be found that the durability performance of the $K_{0.2}Ti_{0.5}Al$ catalyst was significantly improved compared with that of the $Ti_{0.5}Al$ catalyst.

3.2. Pore Structure Analysis. To investigate the differences in the pore structure of different catalysts, the BET results are shown in Figure 6 and Table 1. It can be seen that the IV-type isotherm adsorption−desorption curve, which belonged to a typical mesoporous material, was observed in all catalysts. This indicated that the addition of Na and K hardly changed the physical structure properties of the catalyst itself. It was worth noting that after the addition of alkali metal elements, the pore size distribution curve was obviously shifted to a larger size. In particular, this transformation was most obvious when the Na/K loading was 0.10−0.20. The pore diameter of the blank $Ti_{0.5}Al$ was 4.55 nm. After being doped by alkali metals, they increased to 8.34 nm ($Na_{0.1}Ti_{0.5}Al$) and

https://doi.org/10.1021/acsomega.2c00968
ACS Omega 2022, 7, 13299−13312

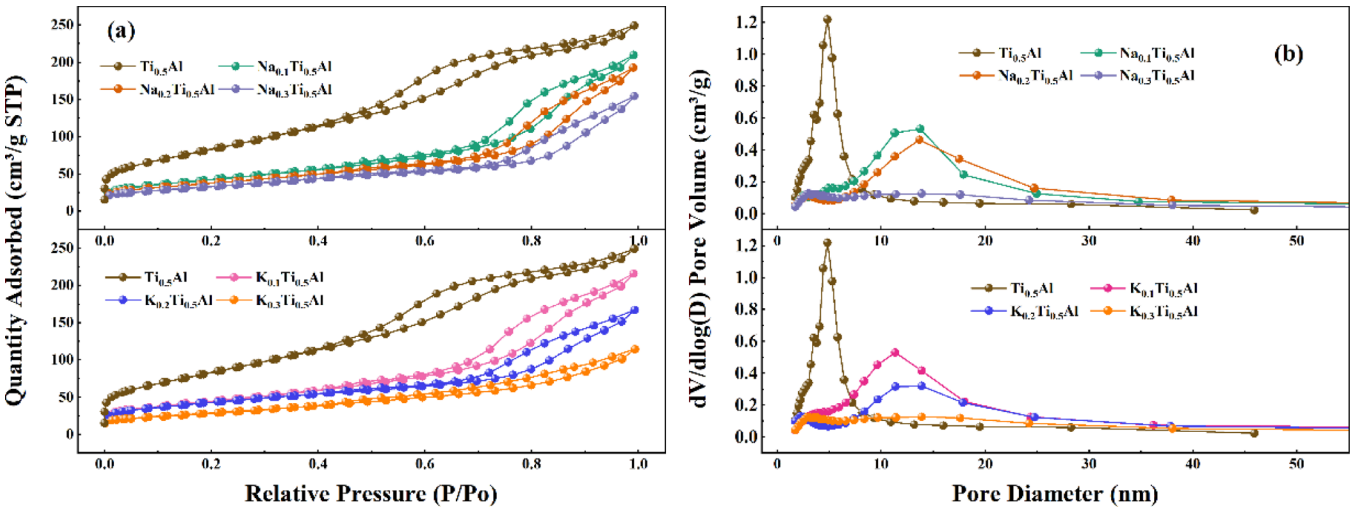

Figure 6. (a) N_2 adsorption isotherms and (b) pore size distribution curve of the $M_xTi_{0.5}Al$ hydrolysis catalyst.

Table 1. Structure Parameters of Different Catalysts[a]

sample	S_{BET} (m^2/g)	V_t (cm^3/g)	W_p (nm)
$Ti_{0.5}Al$	309.37	0.39	4.55
$Na_{0.1}Ti_{0.5}Al$	153.43	0.32	8.34
$Na_{0.2}Ti_{0.5}Al$	135.24	0.30	8.66
$Na_{0.3}/Ti_{0.5}Al$	119.75	0.24	7.93
$K_{0.1}Ti_{0.5}Al$	161.44	0.33	7.62
$K_{0.2}Ti_{0.5}Al$	152.42	0.26	7.48
$K_{0.3}Ti_{0.5}Al$	103.91	0.18	6.37

[a] S_{BET}: specific surface area; V_t: total pore volume; W_p: average pore diameter.

7.62 nm ($K_{0.1}Ti_{0.5}Al$), respectively. It revealed that the pore size increased to a certain extent after doping.

As shown in Table 1, the $Ti_{0.5}Al$ had the largest S_{BET} (309.37 m^2/g) and V_t (0.39 cm^3/g). After alkali metal modification, the S_{BET} of all catalysts was reduced significantly, while the V_t and W_p both increased. Besides, as the load ratio increased, the S_{BET} dropped more. This may be due to the fact that Na^+ and K^+ were preferentially dispersed in the micropores of catalysts, resulting in a decrease in S_{BET}. By comparison, it can be observed that the reduction of the Na-doped catalysts was more than that of the K-doped samples. In addition, it can be found that the S_{BET} variation of the catalysts was inconsistent with the activity test results. This indicated that the enhanced low-temperature hydrolysis activity of the Na/K-doped catalysts was not the result of the increasing active sites caused by the change in specific surface area. It can be assumed that the specific surface area was not the main factor that affected catalytic activity.

3.3. Catalyst Phase Analysis. As we all know, X-ray diffraction (XRD) is a technique that can be used to identify the phase composition and crystallinity of a catalyst, such as the formation of metal oxides and their crystallization on the surface of the catalyst. The XRD results of the hydrolysis catalysts are shown in Figure 7. All catalysts showed typical diffraction peaks of anatase TiO_2 (JCPDS file 21-1272) (25.281, 37.800, 48.049, and 53.890°) and γ-Al_2O_3 X-ray diffraction peaks (JCPDS file 50-0741) (19.347, 45.666, and 66.600°), both of which had the strongest peak intensity. It can be indicated that the main crystal phase of the catalysts hardly changed significantly after the modification.

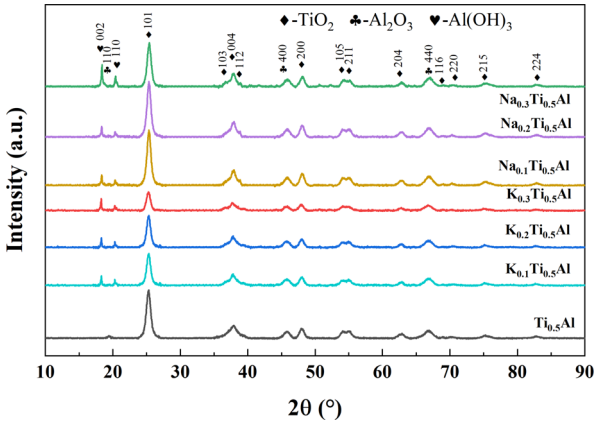

Figure 7. XRD pattern of the hydrolysis catalyst.

After doping the active components Na and K, the diffraction peaks of $Al(OH)_3$ appeared at 18.267 and 20.258° (JCPDS file 70-2038). This may be due to the fact that a large number of −OH groups introduced by Na/K had a strong binding effect with Al^{3+}, leading to the formation of $Al(OH)_3$. In addition, compared with the unmodified $Ti_{0.5}Al$, the peak intensity of the anatase phase TiO_2 of the $K_{0.3}Ti_{0.5}Al$ catalyst was weaker especially at the diffraction angle of 25.281°, indicating that the TiO_2 (110) had a stronger combination with K^+. The crystal grain sizes were all in the range of 10.1−12.1 nm by software calculation, which indicated that the degree of crystallinity of the catalyst carrier had not changed. In Figure 7, the diffraction peaks corresponding to the sodium oxide or potassium oxide were not detected. It could be speculated that these two alkali oxides were well dispersed on the surface of the catalysts, which was conductive to the progress of the COS hydrolysis reaction. The main phases of the catalysts were anatase TiO_2 and γ-Al_2O_3. At the same time, Na and K existed in an amorphous state or were highly dispersed on the catalyst carrier.

3.4. Surface Topography. To investigate the differences in the surface morphology and structure of different catalyst samples, the SEM experiments were carried out for all catalysts. The surface of the $Ti_{0.5}Al$ carrier (Figure 8a) was in the form of fine dispersed particles, without agglomeration, and the overall distribution was relatively flat and uniform. This showed that

https://doi.org/10.1021/acsomega.2c00968
ACS Omega 2022, 7, 13299−13312

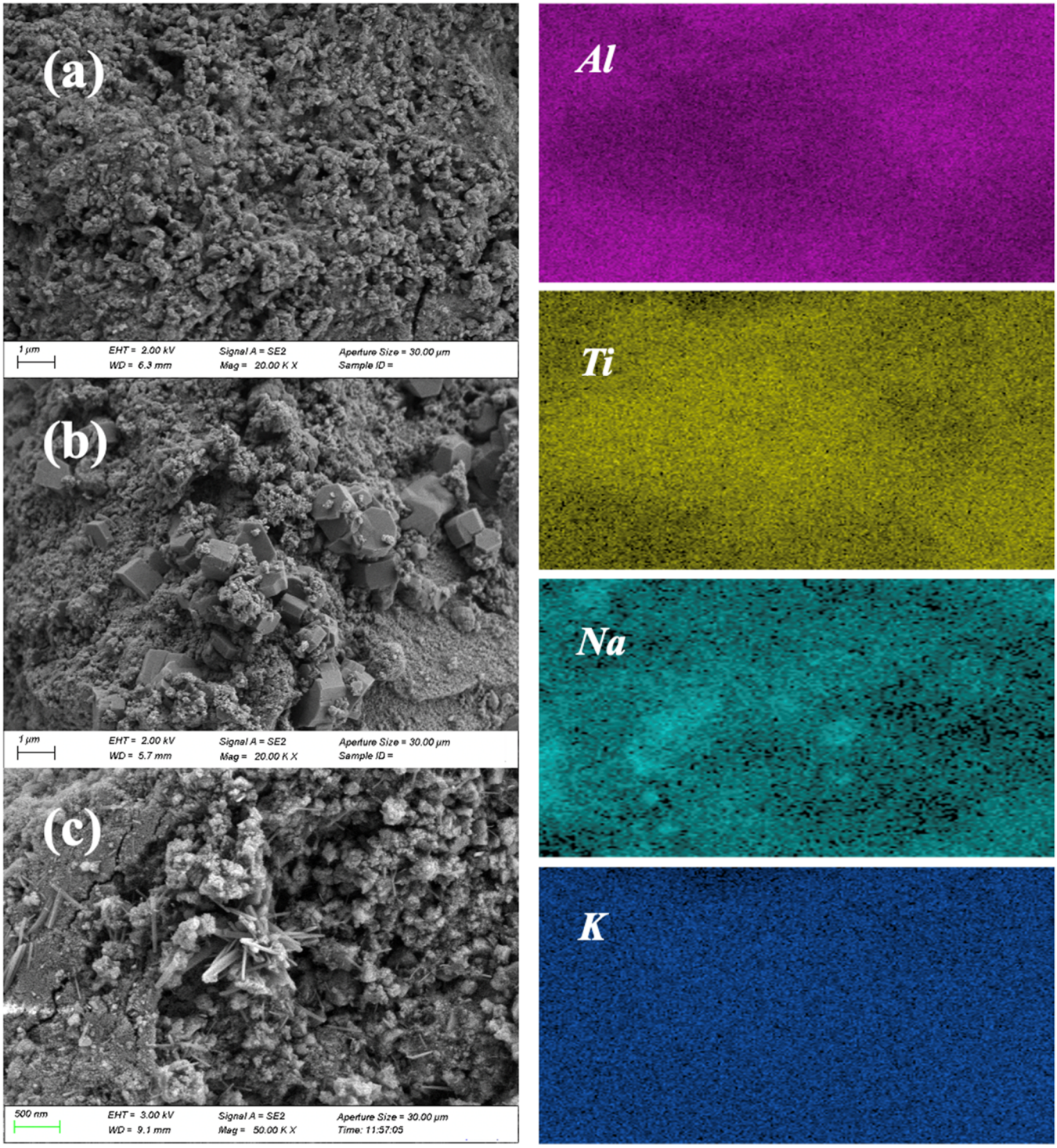

Figure 8. The SEM image and element mappings of (a) $Ti_{0.5}Al$, (b) $Na_{0.2}Ti_{0.5}Al$, and (c) $K_{0.2}Ti_{0.5}Al$.

the components of the $Ti_{0.5}Al$ carrier prepared by the co-precipitation method had great dispersibility and uniformity. The Na-doping sample showed a relatively regular prismatic crystal structure (Figure 8b), while the K-doping sample formed a kind of fine nanorod-like structure (Figure 8c), which can provide more gas contact surfaces for the reaction.[23]

According to the element mapping, it was proved that Na and K are uniformly distributed in the respective samples. BET analysis showed that the pore volume of samples prepared by the deposition of Na_2O and K_2O decreased. It was speculated that the sodium oxide and potassium oxide nanoparticles were more flexibly integrated into the finely dispersed surface pores of $Ti_{0.5}Al$ and bound with Al^{3+}/Ti^{4+} to form a specific crystal phase structure attached to the surface. The results showed that sodium oxide nanoparticles and potassium oxide nanofibers were beneficial to the catalytic and hydrolysis performance of the catalyst.

3.5. Surface Basic Property. *3.5.1. CO_2-TPD Measurements.* Sun et al.[28] pointed out that the hydrolysis of COS is a typical base-catalyzed reaction. The surface alkalinity of the

https://doi.org/10.1021/acsomega.2c00968
ACS Omega 2022, 7, 13299−13312

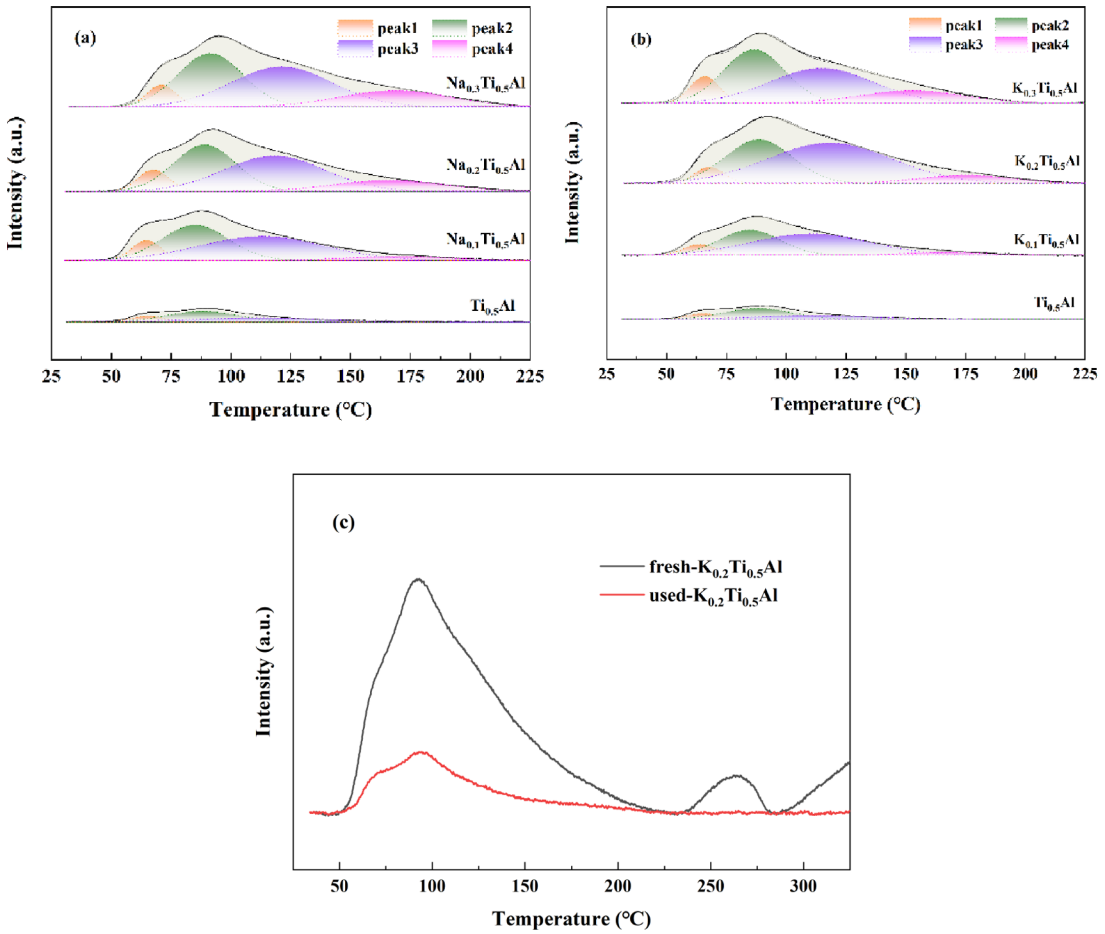

Figure 9. CO_2-TPD results of (a) $Na_xTi_{0.5}Al$ and (b) $K_xTi_{0.5}Al$ hydrolysis catalysts and (c) $K_{0.2}Ti_{0.5}Al$ after the durability test.

Table 2. CO_2-TPD Peak Area Fitting Results of the $M_xTi_{0.5}Al$ Hydrolysis Catalyst

	CO_2 desorption area (relative area)					alkali content ratio (%)	
	weak alkaline site 50−100 °C		moderate alkaline sites 100−225 °C			weak alkaline sites	moderate alkaline sites
catalysts	peak 1	peak 2	peak 3	peak 4	total	50−100 °C	100−225 °C
$Ti_{0.5}Al$	59.72	245.68	150.79		456.18	66.95	33.05
$Na_{0.1}Ti_{0.5}Al$	198.08	798.61	1011.96	133.01	2141.66	46.54	53.46
$Na_{0.2}Ti_{0.5}Al$	226.97	984.65	1213.17	406.88	2831.68	42.79	57.21
$Na_{0.3}Ti_{0.5}Al$	218.34	1186.31	1379.32	609.78	3393.74	41.39	68.61
$K_{0.1}Ti_{0.5}Al$	115.09	506.01	836.41	81.27	1538.78	40.36	59.64
$K_{0.2}Ti_{0.5}Al$	153.72	957.43	1639.17	243.89	2994.21	37.11	62.89
$K_{0.3}Ti_{0.5}Al$	256.93	1079.61	1185.44	426.26	2948.25	45.33	54.67

catalyst played an important role in the adsorption of COS and the subsequent catalytic hydrolysis.[29] For the purpose of determining the effect of Na/K doping on the basic properties of $Ti_{0.5}Al$ catalysts, CO_2-TPD is used to study the surface basicity distribution and alkaline concentration. The results are shown in Figure 9. The band observed between 50 and 225 °C is attributed to the desorption of CO_2 from weak (50−100 °C) and moderate (100−225 °C) basic sites, which are pointed out to be the active center where COS catalytic hydrolysis is carried out.[30,31] It has been proposed that the weak basic sites can be ascribed to the formation of bicarbonates on Brønsted −OH groups and moderate basic sites were attributed to $M^{n+}-O^{2-}$ pairs.[27,32] Obviously, Na^+-O^{2-} and K^+-O^{2-} in Na-$Ti_{0.5}Al$ and K-$Ti_{0.5}Al$ can provide more moderate basic sites compared with $Al^{3+}-O^{2-}$ and $Ti^{4+}-O^{2-}$ in $Ti_{0.5}Al$.

The TPD spectra of all catalysts were measured by Gaussian integration (Table 2). The results showed that the peak areas of the CO_2 desorption curves for $Na_xTi_{0.5}Al$ and $K_xTi_{0.5}Al$ were much larger than those for $Ti_{0.5}Al$, which had the lowest value. Therefore, it can be said that $Na_xTi_{0.5}Al$ and $K_xTi_{0.5}Al$ were more CO_2-philic compared with $Ti_{0.5}Al$, which meant that they had an increased number of alkaline sites. Moreover, the increasing addition of alkali species on catalysts caused the desorption peak to extend toward a higher temperature, indicating that the addition of alkali components increased the number of basic sites together with their basicity, especially peak 1 in the low-temperature region, which was consistent with their low-temperature hydrolysis activity.

CO_2-TPD experiments were also performed on the $K_{0.2}Ti_{0.5}Al$ catalyst that had undergone a durability test. As

https://doi.org/10.1021/acsomega.2c00968
ACS Omega 2022, 7, 13299−13312

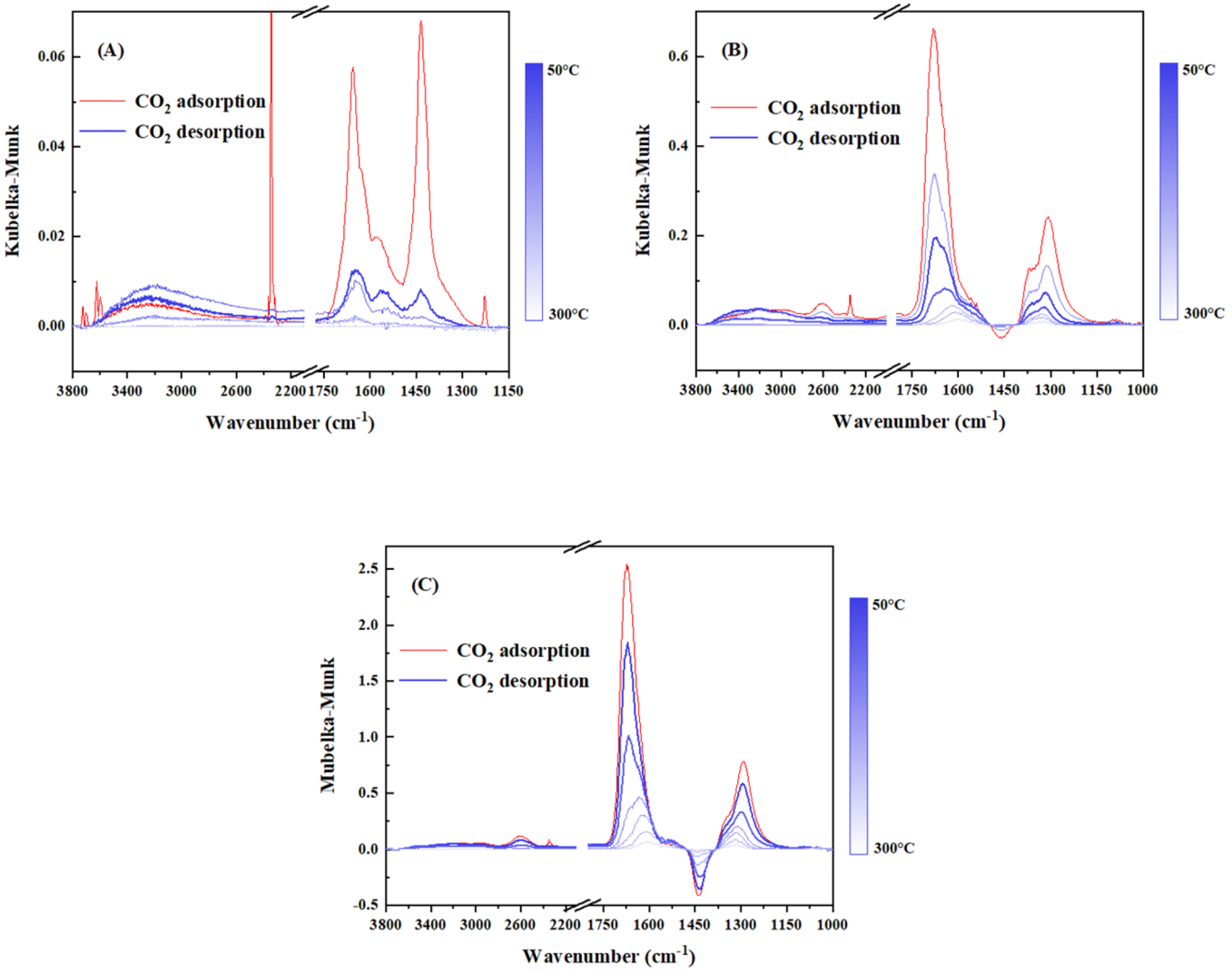

Figure 10. DRIFTS of CO_2 adsorbed and desorbed on (A) $Ti_{0.5}Al$, (B) $Na_{0.2}Ti_{0.5}Al$, and (C) $K_{0.2}Ti_{0.5}Al$ at 50−300 °C.

shown in Figure 9c, a remarkable change in the surface alkalinity of $K_{0.2}Ti_{0.5}Al$ can be observed after 30 h of durability experiments. Not only was the number of surface basic centers reduced, but also the intensity was drastically decreased. This indicates that the loss of surface basicity centers is the direct cause of the decrease in catalytic activity.

3.5.2. CO_2 Adsorption Measurements. To further investigate the hydrolysis mechanism, the adsorption of CO_2 on the samples was studied by in situ DRIFTS. The samples were heat treated at 300 °C in a N_2 atmosphere (100 mL/min) for 1 h, and then they were cooled to 50 °C. The gas flow was switched to 10 vol % CO_2 and 90 vol % N_2 for 30 min. Then the DRIFTS spectra of samples were recorded. Figure 10 shows the DRIFTS spectra of CO_2 adsorption and desorption changes with temperature on the $Ti_{0.5}Al$, $Na_{0.2}Ti_{0.5}Al$, and $K_{0.2}Ti_{0.5}Al$ samples.

Several peaks were detected at 2345, 1665, 1595, 1350, 1300, and 1235 cm^{-1}. The infrared spectrum at 2345 cm^{-1} appeared in all catalysts, which was the asymmetric stretching of CO_2, indicating that the weak physical adsorption of CO_2 happened on all catalysts' surface. Besides, the majority of CO_2 formed surface-bound bicarbonate (1665, 1300, and 1235 cm^{-1}) and carbonate species (1595, 1350, and 1330 cm^{-1}) upon initial adsorption at 50 °C, presumably from Brønsted −OH sites that combine with CO_2 on the catalysts' surface. The intensity of these peaks decreased in the following order: $K_{0.2}Ti_{0.5}Al$ > $Na_{0.2}Ti_{0.5}Al$ > $Ti_{0.5}Al$. The highest peak intensity was observed for $K_{0.2}Ti_{0.5}Al$, indicating that this sample had the strongest CO_2 affinity, which further proved its highest basicity.[33] During the temperature-programmed desorption, bicarbonate signals disappeared by 200 °C, and traces of carbonates were detected up to 300 °C. Based on the thermal properties of the adsorbates formed upon CO_2 adsorption, the basicity, especially weak and moderate basicity, was improved remarkably by K/Na-doping as expected.

3.6. XPS Analysis. XPS was carried out to measure the element content and valence information. The results are shown in Figure 11. The O 1s XPS spectra of the $M_xTi_{0.5}Al$ catalysts are presented in Figure 11a,b, which could be fitted into two peaks according to the binding energy. The peak at 529.9 eV was attributed to lattice oxygen (O_{lat}), while the peak at 531.2 eV can correspond to surface adsorbed oxygen (O_{ads}).[27] Studies have pointed out that due to higher mobility, chemically adsorbed oxygen species are more active than lattice oxygen species. The ratio of O_{ads}/O_{lat} in the $Ti_{0.5}Al$ catalyst was 3.644. After Na and K were doped, the ratios decreased to 1.978 and 1.819, respectively. This reduction might be the result of more adsorbed oxygen to be transformed

https://doi.org/10.1021/acsomega.2c00968
ACS Omega 2022, 7, 13299−13312

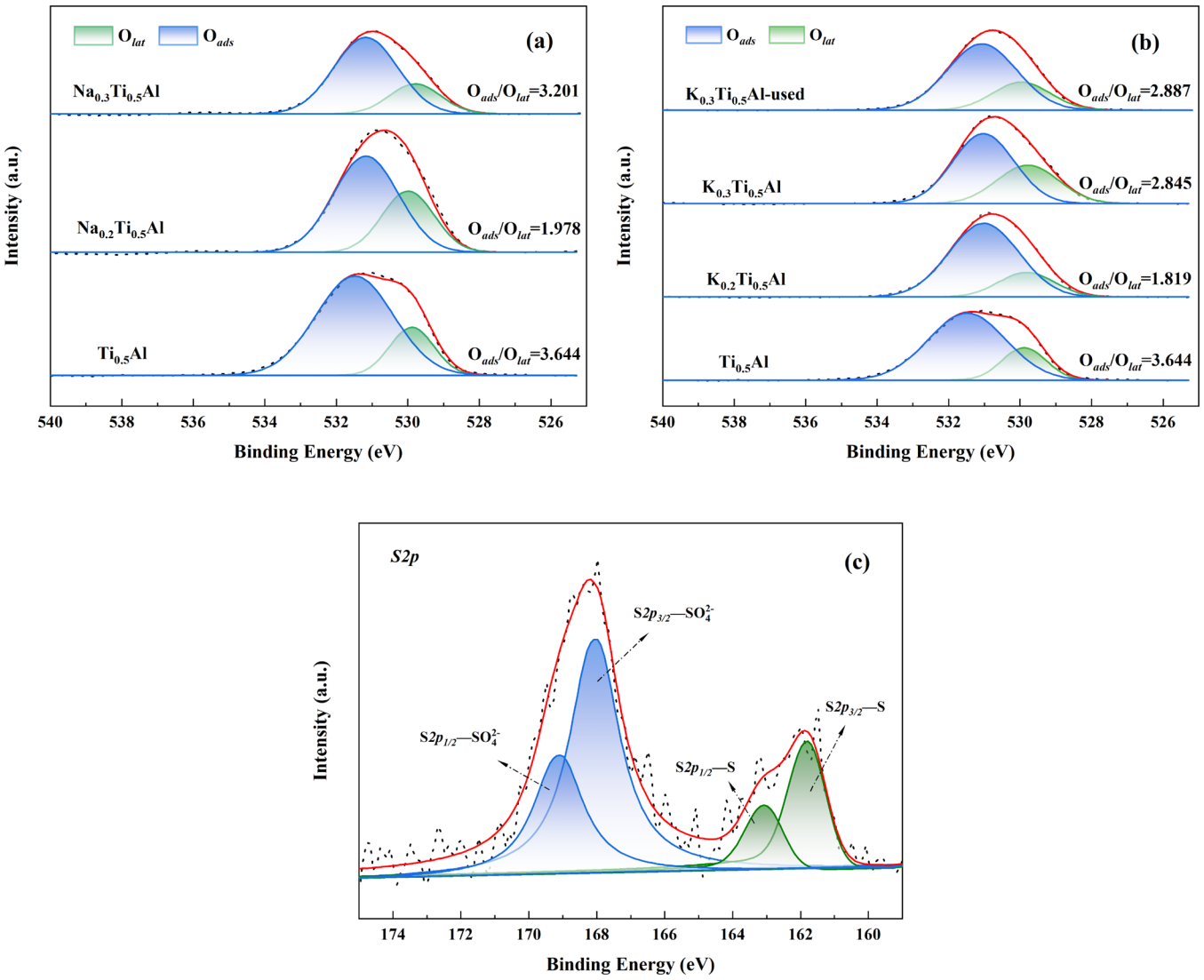

Figure 11. O 1s XPS spectra of (a) $Na_xTi_{0.5}Al$ and (b) $K_xTi_{0.5}Al$ and (c) S 2p of used $K_{0.2}Ti_{0.5}Al$.

into lattice oxygen under the action of alkali metals.[16] Based on the hydrolysis performance, it could be inferred that less adsorbed oxygen was more beneficial to the hydrolysis reaction. At the same time, XPS results also observed that the increased alkali metal loading caused a rise in the O_{ads}/O_{lat} ratio. This may be due to the introduction of more Na^+-O^{2-} and K^+-O^{2-} pairs,[27] which was consistent with the CO_2-TPD results. The higher the ratio of O_{ads}/O_{lat} was, the stronger was the surface oxidation ability. Consequently, the generated H_2S was prone to be oxidized by the active adsorbed oxygen on the surface. This explained why the H_2S yield of the catalysts with high alkali metal loading in the activity evaluation experiment actually decreased.

In addition, the XPS of sulfur species was carried out to further investigate the deactivation mechanism. As presented in Figure 11c, sulfur (around 162.64 eV) and sulfate species (around 168.47 eV) were detected on the used catalyst, which were generated from the oxidation of H_2S (the hydrolysis product of COS) by the surface adsorbed oxygen.[16,34] The oxidation product SO_4^{2-} reacted with K_2O to form K_2SO_4, which consumed the active component and covered the active site on the surface of the catalyst. More importantly, the O_{ads}/O_{lat} of the used catalyst increased (from 1.819 to 2.887). This may be due to the consumption of adsorbed oxygen, which caused a large amount of lattice oxygen to be converted into adsorbed oxygen, which further enhanced the oxidation capacity of the surface. A higher O_{ads}/O_{lat} relative concentration ratio promotes the oxidation of H_2S to sulfate species, thereby hindering the COS hydrolysis reaction. Since more surface oxygen was transformed into lattice oxygen by K-doping (the O_{ads}/O_{lat} decreased from 3.644 to 1.819), consequently less sulfur species could be formed, which is conducive to the long-term catalysis performance.

4. CATALYTIC REACTION MECHANISM

By using in situ DRIFTS, the hydrolysis reaction mechanism of COS over the $M_{0.2}Ti_{0.5}Al$ catalyst was investigated. Before being exposed to the reaction gas, the catalyst was pretreated at 300 °C in N_2 for 1 h. The sample was then cooled to reaction temperature, and the background spectrum was recorded. Then the reaction gas was introduced and the spectrum changes were observed. Therefore, all the characteristic peaks shown in the figure are the result of the interaction between the surface of the catalyst and the gas molecules.

4.1. DRIFTS Analysis of H_2S Adsorption. The H_2S adsorption reaction was studied to explore the role of

https://doi.org/10.1021/acsomega.2c00968
ACS Omega 2022, 7, 13299−13312

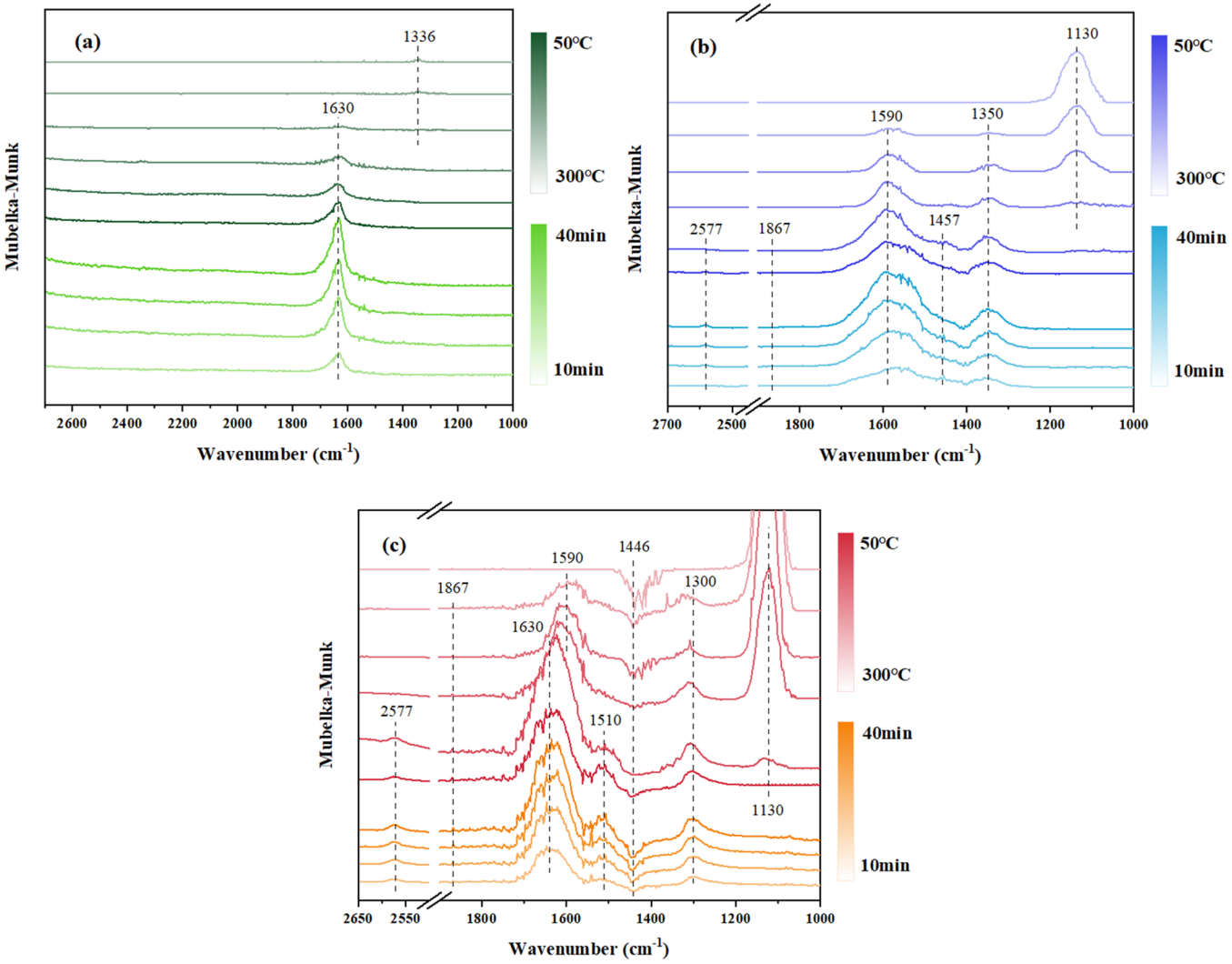

Figure 12. In situ DRIFTS spectra of H_2S adsorption over (a) $Ti_{0.5}Al$, (b) $Na_{0.2}Ti_{0.5}Al$, and (c) $K_{0.2}Ti_{0.5}Al$ (200 ppm H_2S 50−300 °C).

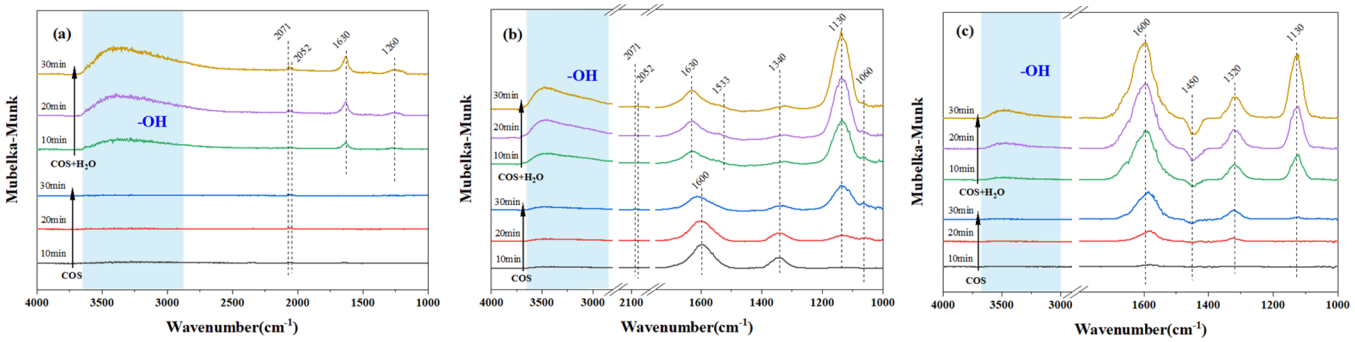

Figure 13. In situ infrared of the reaction of H_2O on the surface of (a) $Ti_{0.5}Al$, (b) $Na_{0.2}Ti_{0.5}Al$, and (c) $K_{0.2}Ti_{0.5}Al$ with preadsorbed COS (500 ppm COS, 75 °C).

hydrolysate (H_2S) on the surface. As shown in Figure 12, several bands were detected at 2577, 1867, 1630, 1510, 1446, and 1300 cm^{-1}. The peak at 2577 cm^{-1} was detected, and the band at 3600-3000 cm^{-1} broadened. The former one might include the contribution from the S−H stretching vibration (M—OH-HSH),[35,36] while the latter was assigned to the surface hydroxyl groups probably derived from eq 5. This indicated the strong interaction between H_2S and the surface −OH groups, providing evidence of the active role of Brønsted −OH sites.[37] The appearance of the band at 1630 cm^{-1} (the molecularly adsorbed H_2O[27,38]) and 1867 cm^{-1} (Al−H stretching vibration) could correspond to the surface reaction of $H_2S + [O] \rightarrow [S] + H_2O$.[39,40] In other words, H_2S was adsorbed onto the surface of samples via a reaction with surface −OH groups to form HS^- and H_2O, as shown in eq 6.

$$H_2S + M - O - M \rightarrow M - SH + M - OH \quad (5)$$

$$H_2S + M - OH \rightarrow M - SH + H_2O \quad (6)$$

https://doi.org/10.1021/acsomega.2c00968
ACS Omega 2022, 7, 13299−13312

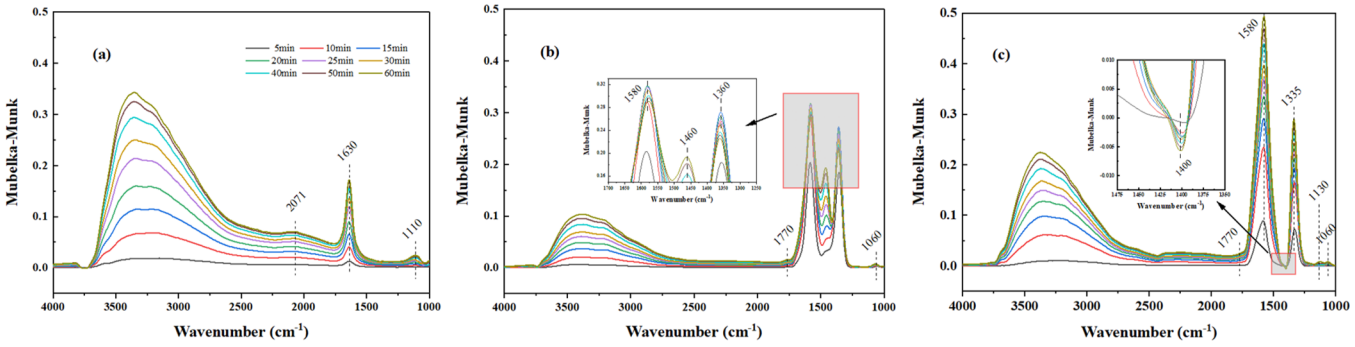

Figure 14. DRIFTS spectra of COS and H_2O simultaneous adsorption over (a) $Ti_{0.5}Al$, (b) $Na_{0.2}Ti_{0.5}Al$, and (c) $K_{0.2}Ti_{0.5}Al$ (500 ppm COS + H_2O, 75 °C).

The infrared spectrum also showed that the band at 1446 cm^{-1} decreased and new bands appeared at 1510 and 1300 cm^{-1}. This showed that SH^- reacted with the strongly bound polydentate carbonate (1446 cm^{-1}) to generate thiocarbonate and bicarbonate (1510 and 1300 cm^{-1}), which were consistent with the DRIFTS phenomenon of H_2S adsorbed on CO_2-treated γ-alumina reported by Lavalley et al.[41] and Yang et al.[42]

The above experimental conclusions showed that the binding force of the $Ti_{0.5}Al$ surface to H_2S was very weak, and only the dissociation of H_2S occurred. After the introduction of alkali metal species, the number of basic groups on the surface increased, and the H_2S adsorption reaction was carried out. This can explain the reason why the H_2S yield in the activity test did not reach 100%: the H_2S generated by the hydrolysis of COS was partially trapped by the basic centers on the surface of the catalyst, and the adsorption oxidation reaction occurred, resulting in a low measured value of H_2S in the outlet gas stream.

4.2. The Adsorption of H_2O after Being Pretreated by COS. Figure 13 depicts the adsorption of H_2O after being pretreated by COS on $M_{0.2}Ti_{0.5}Al$ at 75 °C. After pretreatment by N_2 at 300 °C for 1 h, the reaction chamber was cooled to 75 °C and then the background value at this temperature was recorded. The catalysts were first adsorbed in 500 ppm COS atmosphere for 30 min, and then water vapor was naturally introduced through an impact wash bottle. The spectra progressively changed with the increase of reaction time.

After 30 min of adsorption by COS, only the spectrum of COS (2052 and 2071 cm^{-1}) was detected on the surface of $Ti_{0.5}Al$.[27,38,43] It showed that only weak physical adsorption of COS occurred on the surface. The characteristic vibration peak of COS was also detected on the $Na_{0.2}Ti_{0.5}Al$ surface, while it was not observed on $K_{0.2}Ti_{0.5}Al$. In addition, the vibration peak of carbonates species (1600, 1340, and 1320 cm^{-1}) and other new vibration peaks were also detected on $Na_{0.2}Ti_{0.5}Al$ and $K_{0.2}Ti_{0.5}Al$. The above results indicated that the chemical reaction of COS was carried out on the surface of $Na_{0.2}Ti_{0.5}Al$ and $K_{0.2}Ti_{0.5}Al$ to form carbonate species (1600, 1340, and 1320 cm^{-1}), and at the same time, some physical adsorption of COS also occurred on $Na_{0.2}Ti_{0.5}Al$. Therefore, it can be inferred that the introduction of alkali metal species greatly enhanced the low-temperature adsorption of COS on the surface of the samples, which was beneficial to the progress of the COS hydrolysis reaction.

After introducing the saturated water into the reaction cell, in addition to the characteristic peaks of −OH groups (3700−3000 cm^{-1}) and molecularly adsorbed H_2O (1630 cm^{-1}), the spectrum of $Ti_{0.5}Al$ also showed a broad band at 1260 cm^{-1}, which belonged to =C−O stretching vibration.[39] This may be due to the introduction of H_2O advancing the adsorption of COS on the $Ti_{0.5}Al$ surface and promoting the rupture of the C=S bond in COS to generate the =C−O intermediate. In addition, the characteristic peaks of other species have not been identified. It indicated that the hydrolysis process of COS on the $Ti_{0.5}Al$ surface was relatively slow. This may be due to the lack of weakly basic active sites that made it difficult to provide the activation energy required for the multistep reaction.[21]

As for $Na_{0.2}Ti_{0.5}Al$ (Figure 13b), after 20 min of introducing COS alone, it can be observed that the band at 1600 cm^{-1} gradually migrated to 1630 cm^{-1}, and the intensity of peaks at 1130 and 1060 cm^{-1} increased, while the characteristic peak at 1340 cm^{-1} gradually weakened. This may be due to the initial hydrolysis reaction between COS and the surface to produce a large amount of intermediate carbonate (1600 and 1340 cm^{-1}), which caused the rapid enhancement of the corresponding characteristic peak in a short period of time. Subsequently, the intermediate carbonate was further converted to form C−O (1130 cm^{-1}) and C−S (1060 cm^{-1}) bonds.[39] After saturated water was introduced, the band showed a significant characteristic peak of molecularly adsorbed H_2O (1630 cm^{-1}). In addition, only the peak intensity at 1130 cm^{-1} was enhanced, and no new peaks appeared. Only the identification peak of carbonate (1600 and 1320 cm^{-1}) appeared on $K_{0.2}Ti_{0.5}Al$ without introducing H_2O. Then, a strong peak appeared at 1130 cm^{-1} after the water was introduced, and the other peaks only increased in intensity on the basis of the original bands, which were different from $Na_{0.2}Ti_{0.5}Al$.

In summary, after the catalysts were preadsorbed by COS, the reaction was not significantly changed by the introduction of water. This may be the result of the alkali metal species enriching the OH groups on the surface, and the role of water was to generate hydroxyl groups through the activation of the catalyst surface, supplementing the original hydroxyl groups on the catalyst surface.

4.3. Co-adsorption of COS and H_2O. To further determine the effect of the introduction of alkali metal species on the COS hydrolysis reaction at low temperatures, the in situ infrared experiment of the simultaneous adsorption of COS and H_2O was carried out at 75 °C for 1 h. As shown in Figure 14, after 10 min of reaction, significant hydroxyl band and surface molecules adsorbed H_2O (1630 cm^{-1}) can be observed on the $Ti_{0.5}Al$ surface, and the signal value in the region of 2600−1800 cm^{-1} also had a certain intensity enhancement, making the characteristic peaks in this region covered and

https://doi.org/10.1021/acsomega.2c00968
ACS Omega 2022, 7, 13299−13312

difficult to identify. Furthermore, a slowly growing weak C−O stretching vibration peak appeared at 1110 cm^{-1}. This showed that H_2O was more likely to be adsorbed on the $Ti_{0.5}Al$ surface than COS at low temperatures.[38] A large amount of H_2O covered the active site and inhibited the contact of COS with the surface, which was consistent with the results of the poor low-temperature activity of $Ti_{0.5}Al$.

Compared with $Ti_{0.5}Al$, the adsorption bands after the doping of alkali metal species presented a significant difference. First, the intensity of the hydroxyl band was significantly decreased, and the peak at 1630 cm^{-1} disappeared, indicating that the adsorption of H_2O by the catalyst was weakened. This was conducive to the combination of COS with basic sites on the surface and promoted the progress of the hydrolysis reaction at low temperatures. Second, there were many new vibration peaks detected at 1770, 1580, 1460, 1360, 1335, 1130, and 1060 cm^{-1}. The band at 1770 cm^{-1} related to C═O stretching vibration, and the band at 1060 cm^{-1} belonged to C−S stretching vibration.[29] The bands at 1335 and 1580 cm^{-1} were derived from the symmetric and asymmetric O−C−O stretching vibrations of O−C−O in thiobicarbonate species ($HSCO_2^-$).[27] The band at 1460 cm^{-1} corresponded to the O−H bending vibration in bicarbonate species, and the band at 1360 cm^{-1} referred to the symmetric vibration of O−C−O in bicarbonate species (HCO_3^-). This result revealed that the bicarbonate and hydrogen thiocarbonate species were the main intermediate species.

The above results indicated that after doping with alkali metals, the adsorption of COS on the sample surface was stronger than H_2O, which was conducive to the initial hydrolysis of COS and surface hydroxyl groups to generate intermediate transition species. The possible hydrolysis reaction path of COS occurring on the catalyst surface were shown in Figure 15.

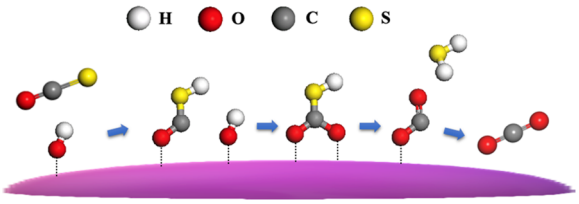

Figure 15. Path speculation of the COS hydrolysis reaction.

5. CONCLUSIONS

In this study, a uniformly dispersed $Ti_{0.5}Al$ composite metal oxide was prepared by the co-precipitation method, and a series of Na/K-doped $Ti_{0.5}Al$ catalysts were prepared by the impregnation method to improve the low-temperature activity and H_2S yield. The results showed that the doping of Na and K significantly enhanced the low-temperature (75−150 °C) activity of the catalysts. CO_2-TPD results proved that weakly basic active centers can be formed more abundantly on the catalyst surface, which were conductive to the adsorption of COS and the remarkable improvement of catalytic performance. Due to the existence of O_{ads}, it was inevitable that the H_2S oxidation reaction occurred. Consequently, the high yield of H_2S in this paper is helpful in proving the weak oxidation ability of the sample surface. The XPS results of the decrease of O_{ads}/O_{lat} on the surface after Na/K doping also help to prove this conclusion. At the same time, a low temperature would also weaken the adsorption and oxidation of H_2S and further reduce the deposition of surface sulfur species, which was conducive to the long-term progress of the catalytic reaction. Finally, in situ infrared was used to explore the mechanism of hydrolysis catalysis. This study showed that the great improvement in low-temperature activity after alkali metal species doping was likely to be caused by two aspects. On the one hand, according to the results of CO_2-TPD, the introduction of alkali metals greatly enhanced the number and alkalinity of weakly basic sites on the surface, which were the sites where the COS hydrolysis reaction occurred. On the other hand, after doping with alkali metals, the adsorption of COS on the sample surface was stronger than H_2O, which was conducive to the initial hydrolysis of COS and surface hydroxyl groups to generate intermediate transition species. This study revealed that thiobicarbonate ($HSCO_2^-$) and bicarbonate (HCO_3^-) are the main reaction intermediates.

AUTHOR INFORMATION

Corresponding Authors

Kai Shen − *Key Laboratory of Energy Thermal Conversion and Control of Ministry of Education, School of Energy and Environment, Southeast University, Nanjing, Jiangsu 210096, China*; orcid.org/0000-0003-3432-6802; Email: shenkai@seu.edu.cn

Yaping Zhang − *Key Laboratory of Energy Thermal Conversion and Control of Ministry of Education, School of Energy and Environment, Southeast University, Nanjing, Jiangsu 210096, China*; orcid.org/0000-0001-5611-3141; Email: amflora@seu.edu.cn

Authors

Yiliang Liu − *Key Laboratory of Energy Thermal Conversion and Control of Ministry of Education, School of Energy and Environment, Southeast University, Nanjing, Jiangsu 210096, China*

Peng Wu − *Key Laboratory of Energy Thermal Conversion and Control of Ministry of Education, School of Energy and Environment, Southeast University, Nanjing, Jiangsu 210096, China*

Guobo Li − *Key Laboratory of Energy Thermal Conversion and Control of Ministry of Education, School of Energy and Environment, Southeast University, Nanjing, Jiangsu 210096, China*

Bo Li − *Jiangsu Langrun Environment Protection Sci & Tech Co., Ltd., Wuxi, Jiangsu 214000, China*

Complete contact information is available at: https://pubs.acs.org/10.1021/acsomega.2c00968

Notes

The authors declare no competing financial interest.

ACKNOWLEDGMENTS

This research did not receive any specific grant from funding agencies in the public, commercial, or not-for-profit sectors.

REFERENCES

(1) Svoronos, P. D. N.; Bruno, T. J. Carbonyl sulfide: A review of its chemistry and properties. *Ind. Eng. Chem. Res.* **2002**, *41*, 5321−5336.
(2) Zhao, S.; Yi, H.; Tang, X.; Ning, P.; Wang, H.; He, D. Effect of Ce-doping on catalysts derived from hydrotalcite-like precursors for COS hydrolysis. *J. Rare Earth.* **2010**, *28*, 329−333.

(3) Zhao, S.; Yi, H.; Tang, X.; Jiang, S.; Gao, F.; Zhang, B.; Zuo, Y.; Wang, Z. The Hydrolysis of Carbonyl Sulfide at Low Temperature: A Review. *Sci. World J.* **2013**, 1.
(4) Li, K.; Song, X.; Ning, P.; Yi, H.; Tang, X.; Wang, C. Energy Utilization of Yellow Phosphorus Tail Gas: Simultaneous Catalytic Hydrolysis of Carbonyl Sulfide and Carbon Disulfide at Low Temperature. *Energy Technol.* **2015**, *3*, 136−144.
(5) Wang, X.; Qiu, J.; Ning, P.; Ren, X.; Li, Z.; Yin, Z.; Chen, W.; Liu, W. Adsorption/desorption of low concentration of carbonyl sulfide by impregnated activated carbon under micro-oxygen conditions. *J. Hazard. Mater.* **2012**, *229-230*, 128−136.
(6) Liu, N.; Wang, X.; Xu, W.; Hu, H.; Liang, J.; Qiu, J. Microwave-assisted synthesis of MoS_2/graphene nanocomposites for efficient hydrodesulfurization. *Fuel* **2014**, *119*, 163−169.
(7) Guo, H.; Tang, L.; Li, K.; Ning, P.; Peng, J.; Lu, F.; Gu, J.; Bao, S.; Liu, Y.; Zhu, T.; et al. Influence of the preparation conditions of MgAlCe catalysts on the catalytic hydrolysis of carbonyl sulfide at low temperature. *RSC Adv.* **2015**, *5*, 20530−20537.
(8) He, E.; Huang, G.; Fan, H.; Yang, C.; Wang, H.; Tian, Z.; Wang, L.; Zhao, Y. Macroporous alumina- and titania-based catalyst for carbonyl sulfide hydrolysis at ambient temperature. *Fuel* **2019**, *246*, 277−284.
(9) Li, X.; Liu, Y.; Wei, X. Technology for carbonyl sulfide removal. *Modern Chem. Ind.* **2004**, *24*, 103−111.
(10) Wang, B.; Lin, Y.; Li, Y.; Wang, J.; Zhu, T. Influencing factors of catalytic hydrolysis of carbonyl sulfide in blast furnace gas. *Clean Coal Technol.* **2021**, *27*, 233−238.
(11) Huang, H. M.; Young, N.; Williams, B. P.; Taylor, S. H.; Hutchings, G. COS hydrolysis using zinc-promoted alumina catalysts. *Catal. Lett.* **2005**, *104*, 17−21.
(12) Jin, H.; An, Z.; Li, Q.; Duan, Y.; Zhou, Z.; Sun, Z.; Duan, L. Catalysts of Ordered Mesoporous Alumina with a Large Pore Size for Low-Temperature Hydrolysis of Carbonyl Sulfide. *Energy Fuel* **2021**, *35*, 8895−8908.
(13) Song, X.; Li, K.; Ning, P.; Wang, C.; Sun, X.; Tang, L.; Ruan, H.; Han, S. Surface characterization studies of walnut-shell biochar catalysts for simultaneously removing of organic sulfur from yellow phosphorus tail gas. *Appl. Surf. Sci.* **2017**, *425*, 130−140.
(14) Li, Q.; Yi, H.; Tang, X.; Zhao, S.; Zhao, B.; Liu, D.; Gao, F. Preparation and characterization of Cu/Ni/Fe hydrotalcite-derived compounds as catalysts for the hydrolysis of carbon disulfide. *Chem. Eng. J.* **2016**, *284*, 103−111.
(15) Song, X.; Ning, P.; Wang, C.; Li, K.; Tang, L.; Sun, X.; Ruan, H. Research on the low temperature catalytic hydrolysis of COS and CS_2 over walnut shell biochar modified by Fe-Cu mixed metal oxides and basic functional groups. *Chem. Eng. J.* **2017**, *314*, 418−433.
(16) Liu, J.; Liu, Y.; Xue, L.; Yu, Y.; He, H. Oxygen Poisoning Mechanism of Catalytic Hydrolysis of OCS over Al_2O_3 at Room Temperature. *Acta Phys.-Chim. Sin.* **2007**, *23*, 997−1002.
(17) Rhodes, C.; Riddel, S. A.; West, J.; Williams, B. P.; Hutchings, G. J. Low-temperature hydrolysis of carbonyl sulfide and carbon disulfide: a review. *Catal. Today* **2000**, *59*, 443−464.
(18) Clark, P. D.; Dowling, N. I.; Huang, M. Conversion of CS_2 and COS over alumina and titania under Claus process conditions: reaction with H_2O and SO_2. *Appl. Catal., B* **2001**, *31*, 107−112.
(19) Liu, Y.; Ju, S.; Wang, Z.; Xu, Y.; Lin, L. Moderate temperature COS hydrolysis activity of γ-Al_2O_3 based catalyst modified by TiO_2. *Chem. Eng. Prog.* **2018**, *37*, 3885−3894.
(20) Liang, L.; Ju, S.; Shen, F.; Liang, M. Investigation on COS hydrolysis over TiO_2 alumina catalyst. In *2nd International Conference on Bioinformatics and Biomedical Engineering, iCBBE 2008*; IEEE, 2008, 3938−3940, DOI: 10.1109/ICBBE.2008.486.
(21) Nimthuphariyha, K.; Usmani, A.; Grisdanurak, N.; Kanchanatip, E.; Yan, M.; Suthirakun, S.; Tulaphol, S. Hydrolysis of carbonyl sulfide over modified Al_2O_3 by platinum and barium in a packed-bed reactor. *Chem. Eng. Commun.* **2021**, *208*, 539−548.
(22) George, Z. M. Effect of catalyst basicity for COS-SO_2 and COS hydrolysis reactions. *J. Catal.* **1974**, *35*, 218−224.
(23) Cao, R.; Ning, P.; Wang, X.; Wang, L.; Ma, Y.; Xie, Y.; Zhang, H.; Qu, J. Low-temperature hydrolysis of carbonyl sulfide in blast furnace gas using Al_2O_3-based catalysts with high oxidation resistance. *Fuel* **2022**, *310*, 122295.
(24) Zhang, Y.; Xiao, Z.; Ma, J. Hydrolysis of carbonyl sulfide over rare earth oxysulfides. *Appl. Catal., B* **2004**, *48*, 57−63.
(25) Zhao, S.; Kang, D.; Liu, Y.; Wen, Y.; Xie, X.; Yi, H.; Tang, X. Spontaneous Formation of Asymmetric Oxygen Vacancies in Transition-Metal-Doped CeO_2 Nanorods with Improved Activity for Carbonyl Sulfide Hydrolysis. *ACS Catal.* **2020**, *10*, 11739−11750.
(26) Thomas, B.; Williams, B. P.; Young, N.; Rhodes, C.; Hutchings, G. J. Ambient temperature hydrolysis of carbonyl sulfide using γ-alumina catalysts: Effect of calcination temperature and alkali doping. *Catal. Lett.* **2003**, *86*, 201−205.
(27) Wei, Z.; Zhang, X.; Zhang, F.; Xie, Q.; Zhao, S.; Hao, Z. Boosting carbonyl sulfide catalytic hydrolysis performance over N-doped Mg-Al oxide derived from MgAl-layered double hydroxide. *J. Hazard. Mater.* **2021**, *407*, 124546.
(28) Sun, X.; Ruan, H.; Song, X.; Sun, L.; Li, K.; Ning, P.; Wang, C. Research into the reaction process and the effect of reaction conditions on the simultaneous removal of H_2S, COS and CS_2 at low temperature. *RSC Adv.* **2018**, *8*, 6996−7004.
(29) Aboulayt, A.; Maugé, F.; Hoggan, P. E.; Lavalley, J. C. Combined FTIR, reactivity and quantum chemistry investigation of COS hydrolysis at metal oxide surfaces used to compare hydroxyl group basicity. *Catal. Lett.* **1996**, *39*, 213−218.
(30) Li, K.; Liu, G.; Wang, C.; Li, K.; Sun, X.; Song, X.; Ning, P. Acidic and basic groups introducing on the surface of activated carbon during the plasma-surface modification for changing of COS catalytic hydrolysis activity. *Catal. Commun.* **2020**, *144*, 106093.
(31) Liu, P.; Derchi, M.; Hensen, E. J. M. Promotional effect of transition metal doping on the basicity and activity of calcined hydrotalcite catalysts for glycerol carbonate synthesis. *Appl. Catal., B* **2014**, *144*, 135−143.
(32) Di Cosimo, J. I.; Díez, V. K.; Xu, M.; Iglesia, E.; Apesteguía, C. R. Structure and surface and catalytic properties of Mg-Al basic oxides. *J. Catal.* **1998**, *178*, 499−510.
(33) Zhao, S.; Tang, X.; He, M.; Yi, H.; Gao, F.; Wang, J.; Huang, Y.; Yang, Z. The potential mechanism of potassium promoting effect in the removal of COS over K/NiAlO mixed oxides. *Sep. Purif. Technol.* **2018**, *194*, 33−39.
(34) Wang, Q.; Zeng, H.; Liang, Y.; Cao, Y.; Xiao, Y.; Ma, J. Degradation of bisphenol AF in water by periodate activation with FeS (mackinawite) and the role of sulfur species in the generation of sulfate radicals. *Chem. Eng. J.* **2021**, *407*, 126738.
(35) Steijns, M.; Koopman, P.; Nieuwenhuijse, B.; Mars, P. The mechanism of the catalytic oxidation of hydrogen sulfide. III. An electron spin resonance study of the sulfur catalyzed oxidation of hydrogen sulfide. *J. Catal.* **1976**, *42*, 96−106.
(36) Toops, T. J.; Crocker, M. New sulfur adsorbents derived from layered IIDRIFTS study of COS and H_2S double hydroxides adsorption. *Appl. Catal., B* **2008**, *82*, 199−207.
(37) Deo, A. V.; Lana, I. G. D.; Habgood, H. W. Infrared studies of the adsorption and surface reactions of hydrogen sulfide and sulfur dioxide on some aluminas and zeolites. *J. Catal.* **1971**, *21*, 270−281.
(38) Liu, Y.; He, H. Experimental and theoretical study of hydrogen thiocarbonate for heterogeneous reaction of carbonyl sulfide on magnesium oxide. *J. Phys. Chem. A* **2009**, *113*, 3387−3394.
(39) Hill, I. M.; Hanspal, S.; Young, Z. D.; Davis, R. J. DRIFTS of Probe Molecules Adsorbed on Magnesia, Zirconia, and Hydroxyapatite Catalysts. *J. Phys. Chem. C* **2015**, *119*, 9186−9197.
(40) Zhang, X.; Tang, Y.; Qiao, N.; Li, Y.; Qu, S.; Hao, Z. Comprehensive study of H_2S selective catalytic oxidation on combined oxides derived from Mg/Al-$V_{10}O_{28}$ layered double hydroxides. *Appl. Catal., B* **2015**, *176-177*, 130−138.
(41) Lavalley, J. C.; Travert, J.; Chevreau, T.; Lamotte, J.; Saur, O. Infrared study of coadsorption of H_2S and CO_2 on γ-alumina. *J. Chem. Soc., Chem. Commun.* **1979**, *4*, 146−148.

https://doi.org/10.1021/acsomega.2c00968
ACS Omega 2022, 7, 13299−13312

(42) Yang, C.; Wang, Y.; Fan, H.; de Falco, G.; Yang, S.; Shangguan, J.; Bandosz, T. J. Bifunctional ZnO-MgO/activated carbon adsorbents boost H_2S room temperature adsorption and catalytic oxidation. *Appl. Catal., B* **2020**, *266*, 118674.
(43) Liu, Y.; Ma, Q.; He, H. Comparative study of the effect of water on the heterogeneous reactions of carbonyl sulfide on the surface of α-Al_2O_3 and MgO. *Atmos. Chem. Phys.* **2009**, *9*, 6273−6286.

https://doi.org/10.1021/acsomega.2c00968
ACS Omega 2022, 7, 13299−13312